Abdominal Radiology
https://doi.org/10.1007/s00261-020-02591-7

PELVIS

Diagnostic value of retrospectively fused $^{64}CuCl_2$ PET/MRI in biochemical relapse of prostate cancer: comparison with fused ^{18}F-Choline PET/MRI, ^{64}CuCl2 PET/CT, ^{18}F-Choline PET/CT, and mpMRI

Francesco Paparo[1] · Alice Peirano[2] · João Matos[2] · Lorenzo Bacigalupo[1] · Umberto Rossi[3] · Ilaria Mussetto[1] · Gianluca Bottoni[4] · Martina Ugolini[5] · Carlo Introini[6] · Filippo Grillo Ruggieri[7] · Gian Andrea Rollandi[1] · Arnoldo Piccardo[4]

Abstract

Purpose To assess the diagnostic value of retrospectively fused PET/MRI by comparing the detection rates (DRs) of fused $^{64}CuCl_2$ PET/MRI vs. fused ^{18}F-Choline PET/MRI in patients with suspected prostatic cancer (PCa) recurrence. The secondary objective was to compare the DRs of fused PET/MRI vs. those of the separate imaging modalities.

Methods We retrospectively evaluated 50 PCa patients with biochemical relapse after radical prostatectomy (RP) or radiotherapy (RT). All patients underwent $^{64}CuCl_2$ PET/CT, ^{18}F-Choline PET/CT, and multiparametric magnetic resonance imaging (mpMRI) within 15 days. Fused $^{64}CuCl_2$-PET/MRI and fused ^{18}F-Choline PET/MRI images were obtained by retrospective co-registration of MRI and PET images. Experienced readers interpreted the images, and the DRs of each imaging modality were assessed.

Results In the patient-based analysis, overall DRs of fused $^{64}CuCl_2$ PET/MRI, fused ^{18}F-Choline PET/MRI, $^{64}CuCl_2$ PET/CT, ^{18}F-Choline PET/CT, and mpMRI were 88%, 68%, 82%, 56%, and 74%, respectively. In the lesion-based analysis, overall DRs of fused $^{64}CuCl_2$ PET/MRI, fused ^{18}F-Choline PET/MRI, $^{64}CuCl_2$ PET/CT, ^{18} F-Choline PET/CT, and mpMRI were 95%, 66%, 87%, 58%, and 71%, respectively.

Conclusions Retrospectively fused PET/MRI is able to overcome the limitations of the separate interpretation of the individual imaging modalities. Fused $^{64}CuCl_2$ PET/MRI provided the highest diagnostic performance in the detection of PCa local relapse.

Keywords Prostate · Cancer · Recurrence · PET · Magnetic resonance imaging

Abbreviations

PCa	Prostate cancer
RP	Radical prostatectomy
RT	Radiotherapy
mpMRI	Multiparametric magnetic resonance imaging
DWI	Diffusion-weighted imaging
DCE	Dynamic contrast-enhanced

Francesco Paparo and Alice Peirano contributed equally to the manuscript.

Electronic supplementary material The online version of this article (https://doi.org/10.1007/s00261-020-02591-7) contains supplementary material, which is available to authorized users.

✉ João Matos
jfgavinadematos@gmail.com

[1] Unit of Radiology, Department of Diagnostic Imaging, E.O. Galliera Hospital, Genoa, Italy

[2] DISSAL – Department of Health Sciences, University of Genoa, Via Antonio Pastore, 1, 16132 Genoa, GE, Italy

[3] Unit of Interventional Radiology, Department of Diagnostic Imaging, E.O. Galliera Hospital, Genoa, Italy

[4] Unit of Nuclear Medicine, Department of Diagnostic Imaging, E.O. Galliera Hospital, Genoa, Italy

[5] Medical Physics Unit, Department of Diagnostic Imaging, E.O. Galliera Hospital, Genoa, Italy

[6] Prostate Unit, Department of Urology, E.O. Galliera Hospital, Genoa, Italy

[7] Unit of Radiotherapy, Department of Diagnostic Imaging, E.O. Galliera Hospital, Genoa, Italy

Published online: 25 May 2020

DR	Detection rate
SUV	Standardized uptake value
PSA	Prostate-specific antigen
PSMA	Prostate-specific membrane antigen
TBRs	Tumor-to-background ratios

Introduction

In patients affected by prostate cancer (PCa) and with evidence of biochemical relapse after first-line curative treatment (i.e., radical prostatectomy [RP] or radiotherapy [RT]), imaging plays a key role in identifying and evaluating the site and extent and of PCa recurrence. Imaging documentation is often required in order to establish the appropriate second-line treatment [1, 2]. In this clinical scenario, the best imaging protocol includes MRI and whole-body PET/CT [2, 3].

Multiparametric magnetic resonance imaging (mpMRI) by means of high-resolution morphological T2-weighted sequences exquisitely depicts the prostatic bed. Morphological sequences are combined with functional MRI techniques, including diffusion-weighted imaging (DWI) and dynamic contrast-enhanced (DCE) perfusion imaging [4]. This approach may already reveal a high number of local PCa recurrences, but the accuracy of mpMRI in the prostatic fossa may be further improved by adding the metabolic information of PET/CT [5–7]. Indeed, the high specificity of PET tracers may help to reach conclusive diagnoses even in doubtful cases in which T2-weighted images, DWI, and DCE-MRI yield contradictory results.

Various tracers, such as ^{18}F-Choline, ^{11}C-Choline ^{68}Ga-PSMA-11, and ^{18}F-Fluciclovine, have been proposed for PET/CT imaging to identify loco-regional and distant metastases. The most effective PET tracer seems to be prostate-specific membrane antigen (PSMA) radio-labeled with ^{68}Ga, which proved to be more sensitive than radio-labeled Choline and Fluciclovine [8]. However, the main limitation of these tracers, including PSMA, is their urinary accumulation. Currently, PET tracers with low urinary excretion are under investigation for clinical implementation. The novel ^{18}F-PSMA-1007 causes less urinary contamination when compared to ^{68}Ga-PSMA-11. In particular, clearance via the urinary tract of ^{18}F-PSMA-1007 is only 1.2% of injected activity [9], and this tracer has shown significant advantages for detecting local relapse and small pelvic lymph nodes that are generally prevalent in patients with biochemical recurrence at very low PSA levels [10]. To this regard, it has to be remembered that there is no accumulation of $^{64}CuCl_2$ in the urinary tract, and that ^{18}F-PSMA-1007 is currently not available in our country. In patients treated with radical prostatectomy, even a small amount of tracer eliminated through the urinary tract may mask or mimic a relapse in the prostatic fossa. Indeed, the vesicourethral anastomosis is a site of urine accumulation and the most common location of local relapse.

Combining PET images with high-resolution mpMRI enables the precise anatomical localization of PET-positive sites even in the case of faint uptake, and allows a more correct interpretation of doubtful findings. The simultaneous acquisition of PET and mpMRI by means of a dedicated PET/MRI scanner is the most direct way to obtain hybrid PET/MRI images, but these novel integrated systems are not widely available, mainly owing to their high cost [11]. A less-expensive compromise is software platforms for retrospective fusion imaging, which allow the integration of two or more imaging modalities that have been acquired at different time points. $^{64}CuCl_2$ PET/CT, which is neither excreted via the urinary tract nor accumulated in the bladder, has recently proved to be an effective tool for the detection of PCa recurrence with excellent diagnostic performance in the assessment of local relapse [11, 12]. This study aimed to determine the detection rate (DR) of retrospectively fused $^{64}CuCl_2$ PET/MRI in a cohort of PCa patients with biochemical recurrence. The secondary objective was to compare the DR of fused $^{64}CuCl_2$ PET/MRI with those of fused ^{18}F-Choline PET/MRI, mpMRI, ^{18}F-Choline PET/CT, and $^{64}CuCl_2$ PET/CT.

Materials and methods

This retrospective study was approved by the local ethics committee and the "Agenzia Italiana del Farmaco," a public agency under the control of the Italian Ministry of Health. Written informed consent was obtained from all participants. The trial was registered in the European Clinical Trial Database (EudraCT number 2014-005140-18).

Study design and inclusion of patients

This retrospective analysis was conducted on the same patient cohort that had been analyzed in a previous study by Piccardo et al. [12], and which included 50 PCa patients presenting with biochemical relapse. Half of the patients (25/50) presented with biochemical relapse after initial treatment, while the other half were included for suspected recurrence after additional or salvage therapy. The clinical and laboratory characteristics of the study population are listed in Table 1. All patients underwent ^{64}CuCl2 PET/CT, ^{18}F-Choline PET/CT, and mpMRI within 15 days of one another.

Table 1 Demographical, clinical, and laboratory characteristics of the study population

Characteristic	Data
Median age (years)	72 (range 52–90)
PSA level (ng/mL)	
Median	1.88 (range 0.24–14.0)
Median PSA doubling time (mo)	4.2 (range 0.9–34)
Median PSA velocity (ng/mL/year)	2.0 (range 0.1-56.4)
Gleason score (*n*)	
3 + 4	12 (24%)
4 + 3	16 (32%)
4 + 4	17 (34%)
4 + 5	1 (2%)
5 + 4	4 (8%)
Treatment at time of biochemical relapse (*n*)	
Radical prostatectomy only	14 (28%)
Radical intent EBRT only	8 (16%)
Hormone therapy only	3 (6%)
Radical prostatectomy + salvage EBRT	8 (16%)
Radical prostatectomy + hormone therapy	4 (8%)
Radical prostatectomy + EBRT + hormone therapy	7 (14%)
Radical intent EBRT + hormone therapy	6 (12%)

Scanning protocols

mpMRI

The mpMRI examinations were acquired by means of a 1.5-T MRI scanner (Signa HDxt™, GE Healthcare, Milwaukee, WI) equipped with an 8-channel pelvic phased-array surface coil. MRI protocol, as described in our previous study [5], included two different axial T2-weighted sequences: the first axial FSE T2-weighted sequence (slice thickness 4 mm, interslice gap 0.4 mm, in plane resolution 0.6 × 0.6 mm) with a large field-of-view (FOV 32 × 32 cm), was set to comprehend the prostate fossa and lymph-node stations of the lower abdomen, including infrarenal paracaval/paraaortic, iliac, and obturator lymph nodes. The second high-resolution oblique axial T2-weighted scan (slice thickness 3–3.5 mm, interslice gap 0.3 mm, FOV 20 × 20) was further oriented perpendicular to the rectoprostatic plane. A gadolinium-enhanced 3-dimensional spoiled gradient echo fat-saturated T1-weighted pulse sequence was set with the same large FOV of the first-mentioned T2-weighted MR sequence.

$^{64}CuCl_2$ PET/CT

The production of experimental $^{64}CuCl_2$ (Sparkle s.r.l™. Macerata, Italy) was approved by "Agenzia Italiana del Farmaco." The radiopharmaceutical was prepared in accordance with Good Manufacturing Practice and administered intravenously to fasting patients (at least 6 h). Whole-body $^{64}CuCl_2$ PET/CT was carried out 60' after the injection of 200-250 MBq of $^{64}CuCl_2$. All PET scans were acquired in 3D mode by a dedicated PET/CT system (Discovery ST™; General Electric Healthcare Technologies, Milwaukee, WI). Considering the relatively low positron production and 511 keV photon emission (yield) of ^{64}Cu, when compared to those of ^{18}F, PET/CT were acquired via 6-min emissions per bed position from the upper neck to the upper thighs, by means of sequential fields of view, each covering 12 cm (matrix of 256 × 256), and visualized on Xeleris™ Workstation version 2.1753 (General Electric, Milwaukee, WI, USA). Low-dose CT was performed for both attenuation correction and anatomical localization.

^{18}F-Choline PET/CT

^{18}F-Choline PET/CT was performed in the fasting state (at least 6 h). An ^{18}F-Choline activity of 200 MBq (IASOCholine™ IASON LabormedizinGesmbh&Co. Kg, Linz, Austria) was administered intravenously; data were acquired 20' after the injection by means of the above-mentioned PET/CT system. PET was performed over an acquisition time of 3' in the same manner as for $^{64}CuCl_2$ PET/CT and visualized on the same workstation. The same CT parameters were also used.

PET/MRI fusion imaging (fused ^{18}F-Choline PET/MRI and fused $^{64}CuCl_2$ PET/MRI)

Co-registration (i.e., multimodal fusion imaging) between MRI and PET images was performed by means of a

dedicated software platform developed for research purposes (Quanta Oncology™, Camelot Biomedical Systems, Genoa, Italy). Using this software platform, a deformable registration technique (employing non-linear transformation and spatially varying deformable models) is used for MRI/PET co-registration, in order to compensate for changes in patient position and local deformations between different imaging datasets (e.g., due to varying degrees of filling of the urinary bladder). In the co-registration process, only T2-weighted MRI sequences are employed [5].

Image interpretation

Patient-based analysis and lesion-based analysis

In the patient-based analysis, the detection rate (DR) was defined as the ability to detect at least one pathological finding in each subject. In lesion-based analysis, the DR was defined as the ability to detect suspicious lesions in relation to the total number of lesions detected by fusion imaging techniques, PET tracers, and mpMRI [13].

mpMRI

All mpMRI studies were reviewed on a dedicated workstation (Advantage Workstation, version 4.6; GE Healthcare) by an abdominal radiologist (with at least 5 years of experience in prostate mpMRI) who was blinded to the results of the PET studies. PCa recurrence was diagnosed when a focal morphological alteration was accompanied by at least one corresponding functional abnormality (on ADC or perfusion maps), or when 2 functional mpMRI criteria were present without a definite morphological lesion. Morphological/size criteria were also adopted to distinguish between benign and malignant lymph nodes (i.e., round shape and short axis of ≥ 8 mm, oval shape and short axis of ≥ 10 mm) [5, 6]. An axial short T1 inversion recovery sequence was used to detect bone metastases.

PET/CT

All PET-CT examinations (including both ^{18}F-Choline PET/CT and $^{64}CuCl_2$ PET/CT studies) were grouped together after anonymization, and each of the two nuclear medicine physicians, blinded to mpMRI results, read half of the cases, which were presented in random order. On ^{18}F-choline PET/CT and $^{64}CuCl_2$ PET/CT, any focal, non-physiological uptake higher than that of the surrounding background level was considered pathological. ^{18}F-choline PET/CT and $^{64}CuCl_2$ PET/CT studies were interpreted visually and semi-quantitatively by using the SUVmax, on a patient-by-patient and lesion-by-lesion basis. Tumor-to-background ratios (TBRs) were determined for each lesion on both $^{64}CuCl_2$ and ^{18}F-Choline images. TBR was established by placing a 2-dimensional region of interest in the pelvis and measuring the SUVmax of the background fat within this area. This value was then used as denominator for TBR calculation. Neither SUVmax nor TBR cut-offs were used to assess PET-positive lesions, although these parameters were employed as a support to visual interpretation. On both ^{18}F-choline PET/CT and $^{64}CuCl_2$ PET/CT, any focal, non-physiologic uptake higher than that of the surrounding background level corresponding on attenuation CT to prostate parenchyma, prostatic fossa, residual seminal vesicles, vesicourethral anastomosis, abdominal/pelvic lymph nodes, and bone was considered pathological. The results of TBR analysis are reported in the supplementary material.

Multimodal fusion imaging

PET/MRI results were interpreted in consensus by the experienced radiologist, who was aware of the PET/CT imaging results, and by the two experienced nuclear medicine physicians, who were aware of the MRI results. On ^{18}F-Choline PET/MRI and $^{64}CuCl_2$ PET/MRI, any focus of non-physiological uptake corresponding at least to any "suspicious" mpMRI finding was deemed suggestive of local recurrence. Any uptake corresponding to mpMRI-detectable abdominal and pelvic lymph nodes was regarded as lymph-node metastasis. Any focal bony uptake corresponding to a pathological finding on mpMRI was regarded as bone metastasis.

Standard of reference

A descriptive standard of reference was employed to provide confirmation of the site of recurrence. Histopathology was obtained by means of transrectal ultrasound-guided biopsy in 7 out of a total of 25 patients with local relapse only (28%). Undetectable PSA values were found after salvage RT in another 4 of the 11 patients with only local recurrence and not previously treated with RT. In the case of lymph-node and distant metastases, we used a multidisciplinary consensus reference based on mpMRI, ^{18}F-Choline PET/CT, and reduction of PSA values after salvage therapy. A median follow-up time of 7 months (range 5–15) was available for each patient.

Statistical analyses

Descriptive statistics included median, minimum, and maximum for continuous data; absolute and relative frequencies for categorical data. DRs were calculated as the ratio between the number of positive patients (or lesions in the case of lesion-based analysis) and the total number of patients (or lesions). The Chi-square test and Fisher's exact test were applied to compare categorical data; the

McNemar test was used for comparing DRs among diagnostic procedures on the same subjects. Results were also stratified according to total PSA levels (≤ 1 ng/mL, 1–2 ng/mL, 2–4 ng/mL, and > 4 ng/mL). Statistical significance was assigned to values of alpha error (two-tailed) lower than 0.05. In the multiple comparisons of Tables 2 and 4, the Bonferroni's corrected *p* value was 0.0125; for Tables 3 and 5, the corrected *p* value for statistical significance was 0.017. All statistical analyses used STATA software™ (StataCorp. 2015. Stata Statistical Software: Release 14. College Station, TX: StataCorp LP.).

Results

Patient-based analysis

In both $^{64}CuCl_2$ and ^{18}F-Choline PET/CT, 11 out of 50 patients showed extrapelvic disease. Six patients had extrapelvic infrarenal paracaval/paraaortic lymph-node metastases, 2 patients had only bone metastases, and the remaining 3 patients presented with bone and extrapelvic lymph-node metastases. Fused $^{64}CuCl_2$ PET/MRI revealed more patients with local recurrence (34/50, 68%) and lymph-node metastases (17/50, 34%) than the other modalities. Specifically, on considering local relapse, the DR of fused $^{64}CuCl_2$ PET/MRI was significantly higher than those of fused ^{18}F-Choline PET/MRI ($p < 0.001$) and mpMRI ($p = 0.004$) (Tables 2 and 3). Figures 1 and 2 depict two cases of local relapse. In the same setting, the DR of fused ^{18}F-Choline PET/MRI was higher than that of ^{18}F-Choline PET/CT ($p = 0.03$), but without reaching the level of statistical significance after Bonferroni's correction. The DR of fused ^{18}F-Choline PET/MRI was significantly lower than $^{64}CuCl_2$ PET/CT ($p = 0.001$) (Table 3).

Lesion-based analysis

Overall, the DR of fused $^{64}CuCl_2$ PET/MRI was higher than that of fused ^{18}F-Choline PET/MRI in detecting PCa lesions ($p < 0.001$); specifically, local recurrences ($p < 0.001$) and lymph-node metastases ($p = 0.002$). Figure 3 depicts an example of nodal metastasis. However, no statistically significant difference was found in the detection of bone lesions (Table 4). Figure 4 is one case of bone metastasis. In addition, DRs of fused $^{64}CuCl_2$ PET/MRI were significantly higher than those of $^{64}CuCl_2$ PET/CT, ^{18}F-Choline PET/CT, and mpMRI (Table 4). Considering the whole amount of

Table 2 Results of the patient-based analysis

Site of disease	$^{64}CuCl_2$ PET/MRI	^{18}F-Choline PET/MRI	*p**	$^{64}CuCl_2$ PET/CT	*p**	^{18}F-Choline PET/CT	*p**	MpMRI	*p**
All positive patients	44/50 (88%)	34/50 (68%)	0.002	41/50 (82%)	0.25	28/50 (56%)	< 0.001	37/50 (74%)	0.02
Local	34/50 (68%)	21/50 (42%)	< 0.001	32/50 (64%)	0.5	15/50 (30%)	< 0.001	25/50 (50%)	0.004
Lymph node	17/50 (34%)	16/50 (32%)	1.0	16/50 (32%)	1.0	15/50 (30%)	0.5	14/50 (28%)	0.25
Bone	5/50 (10%)	5/50 (10%)	1.0	4/50 (8%)	1.0	4/50 (8%)	1.0	5/50 (10%)	1.0

Comparisons among $^{64}CuCl_2$ PET/MRI and all the other imaging modalities. The Bonferroni's corrected *p* level of significance is 0.0125

Table 3 Results of the patient-based analysis

Site of disease	^{18}F-Choline PET/MRI	$^{64}CuCl_2$ PET/CT	*p**	^{18}F-Choline PET/CT	*p**	MpMRI	*p**
All positive patients	34/50 (68%)	41/50 (82%)	0.04	28/50 (56%)	0.03	37/50 (74%)	0.51
Local	21/50 (42%)	32/50 (64%)	0.001	15/50 (30%)	0.03	25/50 (50%)	0.34
Lymph node	16/50 (32%)	16/50 (32%)	1.0	15/50 (30%)	1.0	14/50 (28%)	0.5
Bone	5/50 (10%)	4/50 (8%)	1.0	4/50 (8%)	1.0	5/50 (10%)	1.0

Comparisons among ^{18}F-Choline PET/MRI and all the other imaging modalities. The Bonferroni's corrected *p* level of significance is 0.017

*Exact McNemar Significance Probability

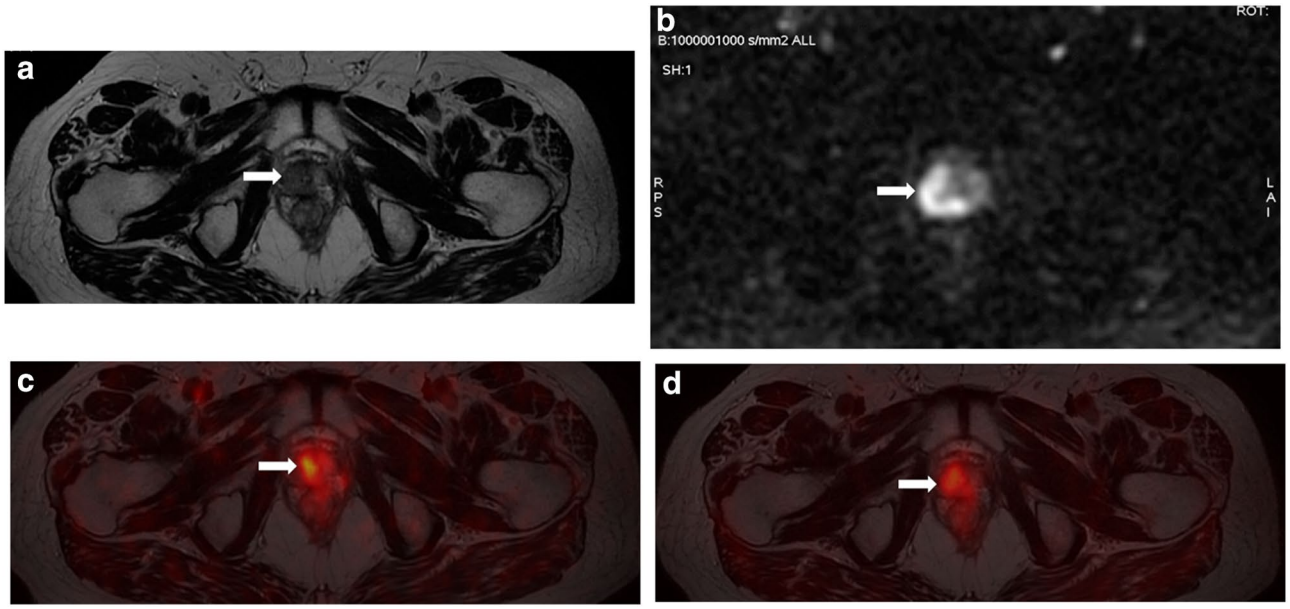

Fig. 1 A 78-year-old patient treated with external beam radiation therapy for prostate cancer Gleason 7 (4 + 3). PSA value of 1.06 ng/mL. The T2w axial MR image **a** shows a large hypointense area in the right peripheral zone extending to the anterior transitional zone (arrow). On the diffusion-weighted image **b** a more circumscribed area of restricted water diffusion is appreciable in correspondence to the right lateral aspect of the peripheral gland (arrow). Both bimodal axial fused $^{64}CuCl_2$ PET/MRI (**c**) and fused ^{18}F-Choline PET/MRI (**d**) show a focal area of tracer uptake in the right lobe of the prostate consistent with local relapse after external beam radiation radiotherapy (arrows)

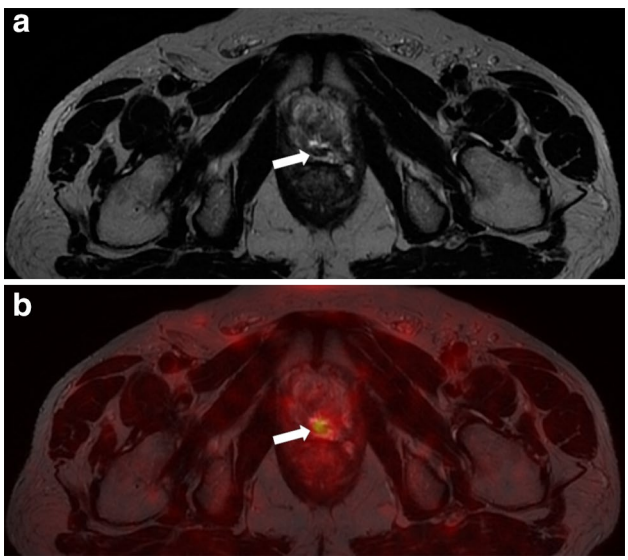

Fig. 2 A 64-year-old man treated with radical prostatectomy for prostate cancer Gleason 9 (4 + 5). PSA value of 5.64 ng/mL. The axial T2w MR image **a** shows a small hypointense nodule in the posterior aspect of the vesicourethral anastomosis (arrow). The bimodal axial fused $^{64}CuCl_2$ PET/MR image **b** allows a precise correspondence to be found between the focal tracer uptake and the perianastomotic nodule (arrow), which was a biopsy-proven local recurrence. In this patient, both ^{18}F-Choline PET/CT and fused ^{18}F-Choline PET/MRI did not show the perianastomotic local recurrence

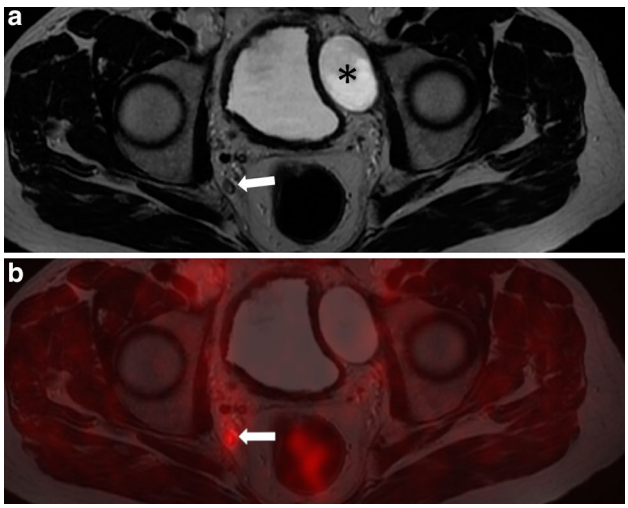

Fig. 3 A 72-year-old male treated with radical prostatectomy for prostate cancer Gleason 7 (4 + 3). PSA value of 1.78 ng/mL. Axial T2w MR image **a** shows a right internal iliac lymph node characterized by an oval shape and short-axis diameter < 7 mm (arrow), which was not considered to be a metastatic site at morphological imaging alone. An oval lymphocele (asterisk) is appreciable in the left lateral aspect of the pelvis, adjacent to the wall of the urinary bladder. The axial fused $^{64}CuCl_2$ PET/MRI **b** demonstrates a focal area of tracer accumulation in correspondence to the internal iliac lymph node, which is consistent with the presence of PCa lymph nodal relapse. In this patient, both ^{18}F-Choline PET/CT and fused ^{18}F-Choline PET/MRI did not reveal any focal tracer accumulation in the pelvis (not shown)

Table 4 Results of the lesion-based analysis

Site of disease	$^{64}CuCl_2$ PET/MRI	^{18}F-Choline PET/MRI	*p**	$^{64}CuCl_2$ PET/CT	*p**	^{18}F-Choline PET/CT	*p**	MpMRI	*p**
All lesions	113/119 (95%)	79/119 (66%)	< 0.001	103/119 (87%)	0.002	69/119 (58%)	< 0.001	84/119 (71%)	< 0.001
Local	44/44 (100%)	21/44 (48%)	< 0.001	40/44 (91%)	0.13	15/44 (34%)	< 0.001	29/44 (66%)	< 0.001
Lymph node	58/61 (95%)	48/61 (79%)	0.002	54/61 (89%)	0.006	45/61 (74%)	0.001	41/61 (67%)	< 0.001
Bone	11/14 (79%)	10/14 (71%)	1.0	9/14 (64%)	0.5	9/14 (64%)	0.5	14/14 (100%)	0.25

Comparisons among $^{64}CuCl_2$ PET/MRI and all the other imaging modalities. The Bonferroni's corrected *p* level of significance is 0.0125

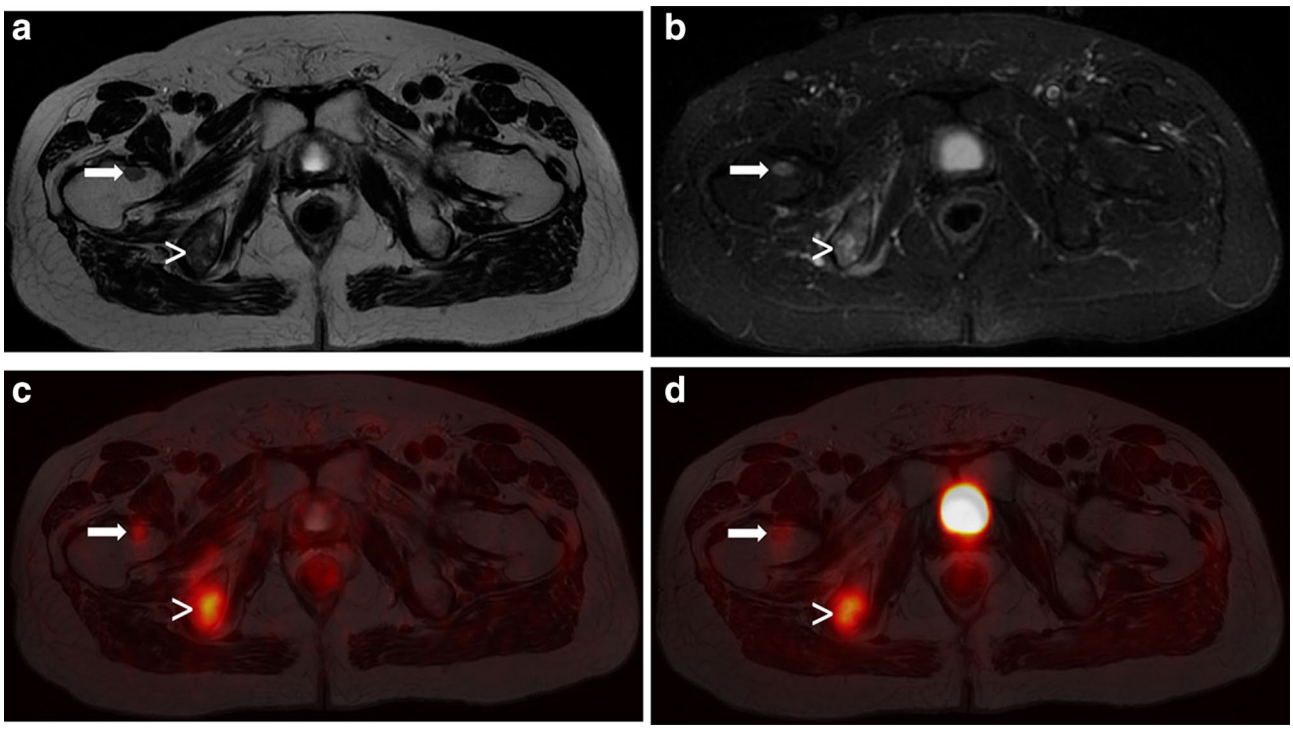

Fig. 4 A 67-year-old male treated with radical prostatectomy for prostate cancer Gleason 8 (4 + 4). PSA value of 3.91 ng/mL. PSA doubling time < 6 months. Axial T2w MR image **a** shows hypointense structural changes in correspondence to the right ischial tuberosity (arrowhead) and a hypointense focal area in the right femoral neck (arrow). The axial STIR image **b** shows the relative signal hyperintensity of these changes when compared with normal adjacent spongy bone (arrow and arrowhead). Both axial fused $^{64}CuCl_2$ PET/MRI (**c**) and fused ^{18}F-Choline PET/MRI (**d**) show focal tracer accumulation in correspondence to the bony lesions (arrow and arrowhead), in keeping with bone metastasis from prostate carcinoma

recurrences, fused ^{18}F-Choline PET/MRI disclosed more lesions than ^{18}F-Choline PET/CT ($p = 0.002$) (Table 5).

PSA-based analysis

When the level of PSA was considered (Fig. 5), fused $^{64}CuCl_2$ PET/MRI identified a higher number of positive patients than fused ^{18}F-Choline PET/MRI in every PSA level range, except for PSA values > 4 ng/mL. In addition, in patients with PSA levels < 2 ng/mL, fused $^{64}CuCl_2$ PET/MRI was the most sensitive imaging procedure.

Discussion

Multimodal PET/MRI fusion imaging is a cornerstone in the field of next-generation diagnostic imaging. Integrated PET/MRI scanners allow anatomical and functional information

Table 5 Results of the lesion-based analysis

Site of disease	^{18}F-Choline PET/MRI	$^{64}CuCl_2$ PET/CT	p*	^{18}F-Choline PET/CT	p*	MpMRI	p*
All lesions	79/119 (66%)	103/119 (87%)	< 0.001	69/119 (58%)	0.002	84/119 (71%)	0.46
Local	21/44 (48%)	40/44 (91%)	< 0.001	15/44 (34%)	0.03	29/44 (66%)	0.06
Lymph node	48/61 (79%)	54/61 (89%)	0.21	45/61 (74%)	0.25	41/61 (67%)	0.09
Bone	10/14 (71%)	9/14 (64%)	1.0	9/14 (64%)	1.0	14/14 (100%)	0.13

Comparisons among ^{18}F-Choline PET/MRI and all the other imaging modalities. The Bonferroni's corrected p level of significance is 0.017

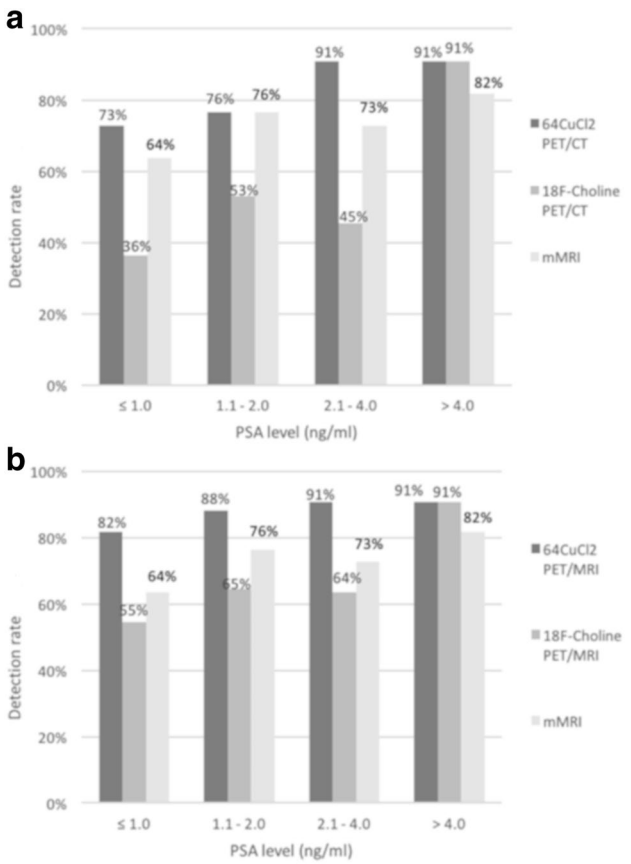

Fig. 5 Bar graph showing the patient-based detection rate (DR) of the various imaging modalities stratified in accordance to different ranges of PSA levels. Image **a** shows the DRs of mpMRI, ^{18}F-Choline PET/CT, and $^{64}CuCl_2$ PET/CT, while image **b** shows the DRs of mpMRI and bimodal fused PET/MRI techniques

from MRI to be combined with the metabolic data provided by the novel radiopharmaceuticals used in PET imaging. The diagnostic value of combined PET/MRI obtained through simultaneous acquisition (i.e., PET/MRI scanner) in PCa patients with biochemical recurrence has been investigated in some previous studies [5–7, 11, 14, 15]. Hybrid imaging overcomes the limitation of the separate assessment of the individual imaging modalities, enabling precise anatomical localization of local recurrence and that of small PET-positive lymph nodes [3]. Unfortunately, the availability of hybrid PET/MRI scanners is still limited to research facilities and has become the standard technique only in resource-rich environments.

Hybrid PET/MRI scanners, by means of dedicated multichannel coils, are able to provide a true multimodal whole-body examination. Retrospectively fused PET/MRI has proved to be a promising alternative to simultaneous hybrid imaging [5].

By using retrospective co-registration of image sets acquired at different time points with variable fields of view (i.e., whole-body PET and pelvic mpMRI), the advantages of fusion imaging are confined to the lower body. In addition, the retrospective co-registration process is technically straightforward (i.e., rigid co-registration) when the fusion imaging platform employs bony landmarks for spatially matching the various image sets. In the rigid co-registration, after an initial pixel resizing, the fusion imaging platform employs translations and rotations of the floating image to obtain a precise juxtaposition on the static reference image.

On the other hand, the computational process becomes more elaborate when anatomical landmarks are soft-tissue structures that may change their position among different examinations (i.e., due to variable degrees of filling of the urinary bladder and rectum, or modified position of the small bowel loops). In this latter case, more advanced co-registration techniques have been developed, which employ localized stretching and elastic deformations of anatomical contours to achieve an accurate fusion of images. This is a field of research. To date, the precision of our software platform in the co-registration process has never been addressed and analyzed in detail, and should be matter of future studies, but we consider that image fusion was obtained with a good precision.

We consider that the comparison between fused $^{64}CuCl_2$ PET/MRI and ^{18}F-Choline PET/MRI has a clinical value.

The results of the present study show that the relatively low detection rate of ^{18}F-Choline PET/CT improved by means of retrospective fusion imaging. However, ^{18}F-Choline PET/MRI was not able to exceed the diagnostic yield of $^{64}CuCl_2$ PET/CT. This is reasonably due to intrinsic features of ^{18}F-Choline, in particular, its route of excretion and a lower TBR when compared to $^{64}CuCl_2$.

The main result of this study emerges from the comparison between the DRs of $^{64}CuCl_2$ PET/MRI and that of $^{64}CuCl_2$ PET/CT in both patient- and lesion-based analyses. In the patient-based analysis, the difference between the overall DR of $^{64}CuCl_2$ PET/MRI (88%) and that of $^{64}CuCl_2$ PET/CT (82%) was evident, but it did not reach the level of statistical significance ($p = 0.25$). This difference in terms of DRs mainly relies in the identification of local recurrences, since the higher spatial and contrast resolution of mpMRI is often able to provide a morphological correlation to any focus of non-physiological tracer uptake. This observation was also confirmed in the lesion-based analysis, which yielded a DR of 100% for $^{64}CuCl_2$ PET/MRI and of 91% for $^{64}CuCl_2$ PET/CT ($p = 0.13$).

The advantages of multimodality fusion imaging were also evident when fused ^{18}F-Choline PET/MRI was compared to conventional ^{18}F-Choline PET/CT. In particular, in the lesion-based analysis, fused ^{18}F-Choline PET/MRI detected six more local recurrences than ^{18}F-Choline PET/CT and three more nodal metastases. These results may be attributed to the lower spatial and contrast resolution of CT in depicting pelvic anatomy and to the renal excretion and urinary accumulation of ^{18}F-Choline, which may hinder the detection of pathological foci of tracer uptake adjacent to the bladder or the urethrovesical anastomosis (Fig. 6).

To this regard, Eiber et al. compared hybrid fused ^{11}C-Choline PET/MRI with ^{11}C-Choline PET/CT in a prospective study and reported significantly different DRs (i.e., 97.3% vs. 64.9%) in detecting local recurrence [16]; findings that are similar to our results.

The underestimation of lymph-node metastases is still a significant limitation of mpMRI. Indeed, only morphological and size criteria are commonly adopted to distinguish between benign and malignant lymph nodes on mpMRI [17]. In the findings from a meta-analysis, investigators reported pooled sensitivity and specificity values of 39% and 82%, respectively, which produces many false negatives on morphological imaging [18]. Therefore, analyzing size-independent metabolic parameters in order to assess the metastatic involvement of lymph nodes has great value in patients with PCa recurrence [19]. Our study showed that multimodality fusion imaging has excellent diagnostic performance in detecting small lymph-node metastases.

In the lesion-based analysis, fused $^{64}CuCl_2$ PET/MRI detected 58/61 nodal metastases (95%) vs. 48/61 (79%) of ^{18}F-Choline PET/MRI ($p = 0.002$). This result may be due to the observation that $^{64}CuCl_2$ has a higher TBR than ^{18}F-Choline. Both retrospectively fused modalities showed to be superior to PET/CT and mpMRI alone. On the other hand, in the patient-based analysis, fused $^{64}CuCl_2$ PET/MRI detected only one more patient with nodal recurrence than fused ^{18}F-Choline PET/MRI.

Some previous studies had already demonstrated the advantages of PET/MRI fusion imaging in detecting nodal metastases, with an impact on patient management even in patients with low PSA values [14, 15, 20].

In one study on ^{18}F-choline hybrid PET/MRI, the DR in patients with PSA ≤ 2 ng/mL was 44% [20]. In our study, fused $^{64}CuCl_2$ PET/MRI displayed the highest overall DR across all PSA intervals, and its diagnostic performance decreased with decreasing PSA values, as expected.

As reported in Tables 3 and 5, considering both the patient- and lesion-based analyses (i.e., all patients and all lesions), no significant difference in terms of detection rate was found between ^{18}F-Choline PET/CT and mpMRI, with p values of 0.46 and 0.51, respectively. A higher performance of mpMRI (near the level of significance) was found only in the lesion-based analysis when considering local relapse. This finding seems to be in contradiction with what was reported in our previous study [5]. This discrepancy may be due to the relevant differences between the populations of patients included in the two studies. Indeed, in the present study, we included 33 patients treated with prostatectomy; on the other hand, all the patients of previous cohort were treated only with external beam RT. The main limitation of both ^{18}F-Choline PET/CT and fused ^{18}F-Choline PET/MRI is related to the low sensitivity of ^{18}F-Choline in detecting PCa local relapse in the prostatic fossa after prostatectomy. Therefore, in this setting, fusion imaging can even reduce the diagnostic yield of the isolated interpretation of mpMRI for the detection of local recurrence; to this regard, it has to be remembered that only morphological T2-weighted sequences are used for image co-registration. This limitation of ^{18}F-Choline is not observed in patients treated with external beam RT, where the urinary accumulation of the tracer is not able to interfere in the assessment of the prostate gland.

The present study had some limitations. First, the retrospective nature of the study makes it prone to selection bias. Second, we employed a descriptive standard of reference, which was not able to provide detailed information on the diagnostic accuracy of each diagnostic technique, including fused $^{64}CuCl_2$ PET/MRI. Therefore, the diagnostic value of each technique was given only in terms of DR. In addition, only a few cases of local recurrences were histopathologically confirmed (i.e., 7 out of 25 patients—28%—). However, the lack of histopathological confirmation as standard of reference is very common in most studies comparing the DRs of different PET tracers in PCa patients with biochemical relapse [5, 8, 14–16,

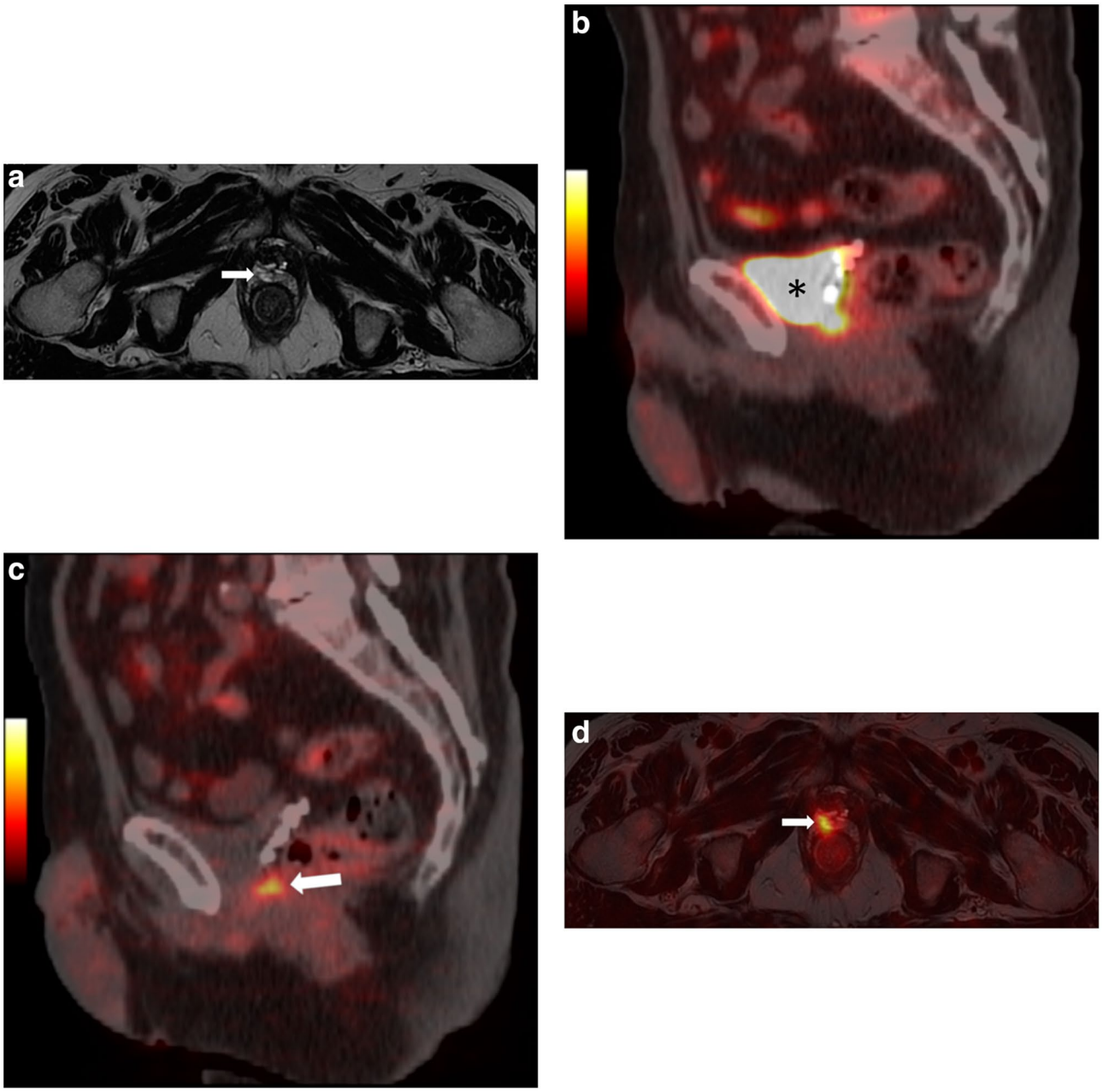

Fig. 6 A 74-year-old male treated with radical prostatectomy for prostate cancer Gleason 7 (4 + 3). PSA value of 1.17 ng/mL. The axial T2w MR image **a** shows a heterogeneous, slightly hyperintense area in correspondence to the posterior aspect of the vesicourethral anastomosis. The sagittal ^{18}F-Choline PET/CT image **b** shows physiological tracer accumulation in the urinary bladder (asterisk), while the corresponding sagittal $^{64}CuCl_2$ PET/CT **c** demonstrates a focal area of tracer accumulation in the rectovesical space (arrow). The axial fused $^{64}CuCl_2$ PET/MRI **d** allows a precise correspondence to be found between the focal tracer uptake and the heterogeneous signal alteration in correspondence to the posterior aspect of the vesicourethral anastomosis (arrow). This case illustrates how the physiological tracer accumulation in the urinary bladder may hinder the identification of perianastomotic local relapse by ^{18}F-Choline PET/CT imaging

20]. Currently, salvage lymph-node dissection is recommended only in selected cases, and the routinely use of transrectal ultrasound-guided biopsy, in particular after RP, is controversial [19]. However, the aim of this study was not to determine the overall diagnostic accuracy of fused $^{64}CuCl_2$ PET/MRI, but to assess and compare the DRs of this hybrid diagnostic approach with other currently accepted imaging procedures.

Retrospectively fused PET/MRI is able to overcome the limitations of the separate assessment/interpretation of the individual imaging modalities. In this pilot study, fused $^{64}CuCl_2$ PET/MRI provided the highest diagnostic

performance in the detection of PCa local recurrence when compared with fused ^{18}F-Choline PET/MRI, $^{64}CuCl_2$ PET/CT, and ^{18}F-Choline PET/CT.

Compliance with ethical standards

Conflict of interest The authors whose names are listed below certify that they have NO affiliations with, or involvement in any organization or entity with any financial interest.

Informed consent The study was approved by the local ethics committee and the "Agenzia Italiana del Farmaco," a public agency under the control of the Italian Ministry of Health. Written informed consent was obtained from all participants.

References

1. Trabulsi EJ, Rumble RB, Jadvar H, et al (2020) Optimum Imaging Strategies for Advanced Prostate Cancer: ASCO Guideline. J Clin Oncol JCO1902757. https://doi.org/10.1200/JCO.19.02757
2. Maurer T, Eiber M, Fanti S, et al (2016) Imaging for Prostate Cancer Recurrence. Eur Urol Focus 2:139–150. https://doi.org/10.1016/j.euf.2016.02.006
3. Perez-Lopez R, Tunariu N, Padhani AR, et al (2019) Imaging Diagnosis and Follow-up of Advanced Prostate Cancer: Clinical Perspectives and State of the Art. Radiology 292:273–286. https://doi.org/10.1148/radiol.2019181931https://doi.org/10.1148/radiol.2019181931
4. Gaur S, Turkbey B (2018) Prostate MR Imaging for Posttreatment Evaluation and Recurrence. Radiol Clin North Am 56:263–275. https://doi.org/10.1016/j.rcl.2017.10.008
5. Piccardo A, Paparo F, Piccazzo R, et al (2014) Value of fused 18F-Choline-PET/MRI to evaluate prostate cancer relapse in patients showing biochemical recurrence after EBRT: preliminary results. Biomed Res Int 2014:103718. https://doi.org/10.1155/2014/103718
6. Paparo F, Piccardo A, Bacigalupo L, et al (2015) Value of bimodal (18)F-choline-PET/MRI and trimodal (18)F-choline-PET/MRI/TRUS for the assessment of prostate cancer recurrence after radiation therapy and radical prostatectomy. Abdom Imaging 40:1772–1787. https://doi.org/10.1007/s00261-014-0345-0
7. Hicks RM, Simko JP, Westphalen AC, et al (2018) Diagnostic Accuracy of 68 Ga-PSMA-11 PET/MRI Compared with Multiparametric MRI in the Detection of Prostate Cancer. Radiology 289:730–737. https://doi.org/10.1148/radiol.2018180788
8. Calais J, Ceci F, Eiber M, et al (2019) (18)F-fluciclovine PET-CT and (68)Ga-PSMA-11 PET-CT in patients with early biochemical recurrence after prostatectomy: a prospective, single-centre, single-arm, comparative imaging trial. Lancet Oncol 20:1286–1294. https://doi.org/10.1016/S1470-2045(19)30415-2
9. Giesel FL, Hadaschik B, Cardinale J, et al (2017) F-18 labelled PSMA-1007: biodistribution, radiation dosimetry and histopathological validation of tumor lesions in prostate cancer patients. Eur J Nucl Med Mol Imaging 44:678–688. https://doi.org/10.1007/s00259-016-3573-4
10. Giesel FL, Knorr K, Spohn F, et al (2019) Detection Efficacy of (18)F-PSMA-1007 PET/CT in 251 Patients with Biochemical Recurrence of Prostate Cancer After Radical Prostatectomy. J Nucl Med 60:362–368. https://doi.org/10.2967/jnumed.118.212233
11. Wetter A, Lipponer C, Nensa F, et al (2014) Evaluation of the PET component of simultaneous [(18)F]choline PET/MRI in prostate cancer: comparison with [(18)F]choline PET/CT. Eur J Nucl Med Mol Imaging 41:79–88. https://doi.org/10.1007/s00259-013-2560-2
12. Piccardo A, Paparo F, Puntoni M, et al (2018) (64)CuCl2 PET/CT in Prostate Cancer Relapse. J Nucl Med 59:444–451. https://doi.org/10.2967/jnumed.117.195628
13. Schwenck J, Rempp H, Reischl G, et al (2017) Comparison of 68 Ga-labelled PSMA-11 and 11C-choline in the detection of prostate cancer metastases by PET/CT. Eur J Nucl Med Mol Imaging 44:92–101. https://doi.org/10.1007/s00259-016-3490-6
14. Riola-Parada C, Carreras-Delgado JL, Pérez-Dueñas V, et al (2018) (18)F-choline PET/MRI in suspected recurrence of prostate carcinoma TT - PET/RM con (18)F-colina en la sospecha de recurrencia del carcinoma de próstata. Rev Esp Med Nucl Imagen Mol 37:296–301. https://doi.org/10.1016/j.remn.2018.04.001
15. Zhang TW, Kassam Z, Rachinsky I, et al (2015) 18F-Fluorocholine (18F-FCH) Hybrid PET/MRI in the Evaluation of Men With Suspected Prostate Cancer Recurrence Following Definitive Local Therapy. Int J Radiat Oncol 93:E214. https://doi.org/10.1016/j.ijrobp.2015.07.1089
16. Eiber M, Rauscher I, Souvatzoglou M, et al (2017) Prospective head-to-head comparison of (11)C-choline-PET/MR and (11)C-choline-PET/CT for restaging of biochemical recurrent prostate cancer. Eur J Nucl Med Mol Imaging 44:2179–2188. https://doi.org/10.1007/s00259-017-3797-y
17. Turkbey B, Rosenkrantz AB, Haider MA, et al (2019) Prostate Imaging Reporting and Data System Version 2.1: 2019 Update of Prostate Imaging Reporting and Data System Version 2. Eur Urol 76:340–351. https://doi.org/10.1016/j.eururo.2019.02.033
18. Hövels AM, Heesakkers RAM, Adang EM, et al (2008) The diagnostic accuracy of CT and MRI in the staging of pelvic lymph nodes in patients with prostate cancer: a meta-analysis. Clin Radiol 63:387–395. https://doi.org/10.1016/j.crad.2007.05.022
19. Wibmer AG, Burger IA, Sala E, et al (2016) Molecular Imaging of Prostate Cancer. Radiographics 36:142–159. https://doi.org/10.1148/rg.2016150059
20. Achard V, Lamanna G, Denis A, et al (2019) Recurrent prostate cancer after radical prostatectomy: restaging performance of 18F-choline hybrid PET/MRI. Med Oncol 36:67. https://doi.org/10.1007/s12032-019-1291-z